Anelastic Internal Wave Packet Evolution and Stability

HAYLEY V. DOSSER* AND BRUCE R. SUTHERLAND

University of Alberta, Edmonton, Alberta, Canada

(Manuscript received 14 April 2011, in final form 13 June 2011)

ABSTRACT

As upward-propagating anelastic internal gravity wave packets grow in amplitude, nonlinear effects develop as a result of interactions with the horizontal mean flow that they induce. This qualitatively alters the structure of the wave packet. The weakly nonlinear dynamics are well captured by the nonlinear Schrödinger equation, which is derived here for anelastic waves. In particular, this predicts that strongly nonhydrostatic waves are modulationally unstable and so the wave packet narrows and grows more rapidly in amplitude than the exponential anelastic growth rate. More hydrostatic waves are modulationally stable and so their amplitude grows less rapidly. The marginal case between stability and instability occurs for waves propagating at the fastest vertical group velocity. Extrapolating these results to waves propagating to higher altitudes (hence attaining larger amplitudes), it is anticipated that modulationally unstable waves should break at lower altitudes and modulationally stable waves should break at higher altitudes than predicted by linear theory. This prediction is borne out by fully nonlinear numerical simulations of the anelastic equations. A range of simulations is performed to quantify where overturning actually occurs.

1. Introduction

As a direct consequence of the conservation of momentum, internal gravity waves grow in amplitude as they propagate upward through the atmosphere's decreasing background density (Eliassen and Palm 1961; Bretherton 1966). This anelastic growth and the critical-level interactions were considered by Lindzen (1981) to be the most important mechanisms by which internal waves ultimately break and irreversibly deposit their momentum to the background. In particular, that work used linear theory to predict where internal waves would grow to such large amplitudes that they would overturn and thereafter continually deposit momentum so as to maintain a critical overturning amplitude. This heuristic was incorporated into so-called gravity wave drag schemes used to capture momentum transport and deposition by subgrid-scale internal waves in general circulation models (McFarlane 1987; Palmer et al. 1986; Scinocca and McFarlane 2000). Their inclusion improved predictions of the mean zonal winds and temperatures in the middle atmosphere (McLandress 1998).

Although efficient and intuitive, it is questionable to use linear theory to make predictions concerning the nonlinear process of breaking. Here we focus specifically on the nonlinear dynamics that influence the evolution of a quasi-monochromatic wave packet that grows anelastically to moderately large and ultimately overturning amplitudes.

A wave packet that is horizontally periodic and vertically localized induces a transient horizontal wind that is analogous to the ''Stokes drift'' for surface waves. We refer to this here as the ''wave-induced mean flow.'' Through quasi-linear numerical simulations Dunkerton (1981) showed that the wave-induced mean flow can modify the background flow, thereby changing the breaking height of the waves. Later studies confirmed that large-amplitude wave packets behaved qualitatively differently than the predictions of linear theory because of nonlinear interactions with the mean flow near a critical level (Fritts and Dunkerton 1984). These interactions, referred to as ''self-acceleration,'' resulted in changes to the phase speed, vertical wavenumber, and group velocity associated with the wave packet. These quantities increased at the wave packet's leading edge and decreased at its trailing edge. This caused the wave packet envelope to

* Current affiliation: Applied Physics Laboratory, University of Washington, Seattle, Washington.

Corresponding author address: Bruce Sutherland, Depts. of Physics and Earth & Atmospheric Sciences, 4-183 CCIS, University of Alberta, Edmonton, AB T6G 2E1, Canada.
E-mail: bruce.sutherland@ualberta.ca

DOI: 10.1175/JAS-D-11-097.1

spread vertically, modifying it to such a degree that it could propagate beyond its original critical level.

Even in the absence of background flow, sufficiently large-amplitude internal wave packets can induce a mean flow that Doppler-shifts the waves so as to change the structure of the wave packet itself. This feedback has been identified as the primary mechanism governing the weakly nonlinear evolution of a Boussinesq wave packet (Grimshaw 1975; Akylas and Tabaei 2005; Sutherland 2006b) and of a non-Boussinesq internal wave packet in a liquid (Dosser and Sutherland 2011).

One expression for the wave-induced mean flow arises from Hamiltonian fluid mechanics as the pseudomomentum per unit mass (Scinocca and Shepherd 1992) or through simple consideration of the circulation around a loop formed by an isentrope before and after it is displaced by a wave (e.g., see Sutherland 2010, section 3.4). Explicitly, for a horizontally periodic wave with vertical displacement $\xi(x, z, t)$ and spanwise vorticity $\xi(x, z, t)$, its wave-induced mean flow is

$$U(z,t) \equiv -\langle \xi\zeta \rangle. \tag{1}$$

Here the angle brackets denote averaging over one horizontal wavelength. This order amplitude-squared form of the wave-induced mean flow is accurate for small-amplitude waves and has been shown to be a good approximation for Boussinesq waves close to breaking amplitudes (Sutherland 2001, 2006b).

The evolution of a weakly nonlinear Boussinesq internal gravity wave packets in uniformly stratified fluid in a background that is stationary in the absence of waves is prescribed by the nonlinear Schrödinger equation (Akylas and Tabaei 2005; Sutherland 2006b)

$$\partial_t A + c_{gz}\partial_z A = \imath\frac{1}{2}\omega_{mm}\partial_{zz}A - \imath kUA, \tag{2}$$

in which $A(z, t)$ is the amplitude envelope of a quasi-monochromatic wave packet with wavenumber vector $\mathbf{k} = (k, m) = (k, m)$ and frequency ω. The second term on the left-hand side of (2) describes the vertical translation of the wave at the group speed $c_{gz} = \omega_m$, in which the subscript denotes the derivative of the frequency ω with respect to the vertical wavenumber m. The first (linear) term on the right-hand side of (2) describes the dispersion of the wave packet and the second (nonlinear) term describes the Doppler-shifting of the waves by the wave-induced mean flow $U \propto |A|^2$.

The sign of the coefficients of the linear and nonlinear terms on the right-hand side of (2) determine the modulational stability of the wave packet (Whitham 1974; Phillips 1981). In particular, because kU is positive for Boussinesq wave packets they are modulationally stable if their frequency is sufficiently small that $\omega_{mm} > 0$. Explicitly, this occurs if $\omega < N/\sqrt{2}$, in which N is the buoyancy frequency. Such wave packets broaden faster than the rate predicted by linear dispersion and their amplitude decreases more rapidly. In contrast, Boussinesq internal wave packets are modulationally unstable if $N/\sqrt{2} < \omega < N$. If sufficiently large, the amplitude envelope of these waves narrows and the peak amplitude increases. The analogous phenomenon that occurs for a packet of surface waves in deep water is known as Benjamin–Feir instability (Benjamin and Feir 1967). If their finite-amplitude evolution is well described by the surface-wave equivalent equation to (2), the amplitude growth reaches a peak and then decreases as energy is transferred to waves in sideband frequencies. The process then repeats through the process of Fermi–Pasta–Ulam recurrence (Fermi et al. 1974). By adding higher-order linear and nonlinear terms to the nonlinear Schrödinger equation for Boussinesq waves, the recurrence phenomena were found to be modified through the deceleration of the wave packet's vertical advance (Sutherland 2006b).

Likewise, the modulational stability and symmetry breaking of modulationally unstable wave packets were observed in the study of internal waves moving upward through a non-Boussinesq liquid (Dosser and Sutherland 2011). The weakly nonlinear and fully nonlinear models study the anelastic-like dynamics of amplitude growth resulting from significantly decreasing background density with height. However, the internal energy and mass conservation equations were those for an incompressible liquid. Because the amplitude grew as the wave packet propagated to greater heights, even waves with initially small amplitudes evolved to become weakly and then fully nonlinear. By growing faster than exponentially, modulationally unstable wave packets were found to overturn below the height predicted by linear theory. Conversely, modulationally stable wave packets overturned above the predicted overturning height.

One purpose of the work presented here is to examine the weakly nonlinear evolution of anelastic internal wave packets in a gas, as appropriate for the study of atmospheric internal waves. This is done in section 2 where we develop an alternate derivation of the wave-induced mean flow and then derive the fourth-order accurate nonlinear Schrödinger equation for anelastic waves. Its solution demonstrates the early stages in the evolution of modulationally unstable, stable, and marginally unstable wave packets. In section 3 we describe the fully nonlinear numerical model used to simulate wave packets in an anelastic gas. Its results are first compared with the predictions of the nonlinear Schrödinger equation, demonstrating both the validity of the assumptions going into the weakly nonlinear theory and the accuracy of the

nonlinear code. In that section we go on to characterize where overturning of wave packets first occurs relative to the breaking heights predicted by linear theory. The implications of these results for gravity wave drag parameterizations are discussed in section 4.

2. Weakly nonlinear evolution

The theory developed here for the linear and weakly nonlinear evolution of anelastic internal wave packets assumes that the background in the absence of waves is isothermal (uniformly stratified) and stationary. The influence of Coriolis forces is neglected. The quasi-monochromatic wave packets themselves are assumed to exist in the x–z plane, being horizontally periodic but having nontrivial structure in the vertical. We begin by developing formulas for the wave-induced mean flow and use these to develop a nonlinear Schrödinger (NLS) equation describing the weakly nonlinear evolution of the wave packets. Finally, solutions are presented for three circumstances demonstrating the modulational stability and instability of the wave packets as they depend on vertical wavenumber.

a. Wave-induced mean flow

Whether linear or nonlinear, horizontally periodic wave packets induce a horizontal mean flow $U \equiv U(z, t)$. This follows immediately from writing the horizontal momentum equation in flux form and averaging in x over one horizontal wavelength:

$$\frac{\partial}{\partial t}(\rho U) = -\frac{\partial}{\partial z}(\overline{\rho}\langle uw\rangle). \tag{3}$$

Here $\overline{\rho}(z)$ is the background density; u and w denote fluctuation horizontal and vertical velocities, respectively, associated with the waves; and the angle brackets denote averaging over one horizontal wavelength.

The momentum flux $\overline{\rho}\langle uw\rangle$ of upward-propagating waves is smaller at the wave packet's leading edge than near its center. It is this divergence in the momentum flux resulting from vertical variations of the amplitude envelope that leads to transient acceleration and deceleration of the background horizontal flow as the wave packet passes by.

Specifically, consider the case of an isothermal atmosphere with exponentially decreasing background density given by

$$\overline{\rho}(z) = \rho_0 \exp(-z/H), \tag{4}$$

in which H is the density scale height. We may denote the fluctuation velocity components associated with a small-amplitude, horizontally periodic, quasi-monochromatic anelastic internal wave packet by

TABLE 1. The dispersion and polarization relations for plane anelastic internal waves in uniformly stratified, stationary fluid. The relationship between the mass-streamfunction amplitude $A_{\psi 0}$ and the amplitudes of other fields including the horizontal u and vertical w velocity, the vorticity ζ, the vertical displacement ξ, and the fluctuation potential temperature θ and density ρ, in which $\varphi = kx + mz - \omega t$ and $K^2 = k^2 + m^2 + 1/(4H^2)$. Throughout, the frequency and horizontal wavenumber are taken to be positive, corresponding to rightward propagating waves. For upward propagating waves, $m < 0$.

Field	Relation to $A_{\psi 0}$
$\psi = \mathrm{Re}(\rho_0 A_{\psi 0} e^{i\varphi} e^{-z/2H})$	$A_{\psi 0}$
$u = \mathrm{Re}(A_{u0} e^{i\varphi} e^{z/2H})$	$A_{u0} = \left(-\imath m + \frac{1}{2H}\right) A_{\psi 0}$
$w = \mathrm{Re}(A_{w0} e^{i\varphi} e^{z/2H})$	$A_{w0} = \imath k\, A_{\psi 0}$
$\zeta = \mathrm{Re}(A_{\zeta 0} e^{i\varphi} e^{z/2H})$	$A_{\zeta 0} = K^2 A_{\psi 0}$
$\xi = \mathrm{Re}(A_{\xi 0} e^{i\varphi} e^{z/2H})$	$A_{\xi 0} = -\frac{K}{N} A_{\psi 0}$
$\theta = \mathrm{Re}(A_{\theta 0} e^{i\varphi} e^{z/2H})$	$A_{\theta 0} = \overline{\theta}' \frac{K}{N} A_{\psi 0}$
$\rho = \mathrm{Re}(A_{\rho 0} e^{i\varphi} e^{-z/2H})$	$A_{\rho 0} = -\frac{\rho_0}{H_\theta} \frac{K}{N} A_{\psi 0}$
Dispersion relation and its derivatives	
$\omega = Nk/K$	
$c_{gz} = \omega_m = -Nkm/K^3$	
$\omega_{mm} = -N(3m^2 - K^2)k/K^5$	
$\omega_{mmm} = 3N(3K^2 - 5m^2)km/K^7$	
Wave-induced mean flow	
$U = \frac{1}{2}\frac{K^3}{N}\lvert A_{\psi 0}\rvert^2 e^{z/H} = \frac{1}{2} NK \lvert A_{\xi 0}\rvert^2 e^{z/H}$	

$$u(x, z, t) = \mathrm{Re}\{A_u \exp[\imath(kx + mz - \omega t)] e^{z/2H}\},$$
$$w(x, z, t) = \mathrm{Re}\{A_w \exp[\imath(kx + mz - \omega t)] e^{z/2H}\}, \tag{5}$$

in which Re denotes the real part. The amplitude envelopes A_u and A_w are (possibly complex-valued) functions of vertical space and time and so the momentum flux $\overline{\rho}\langle uw\rangle = (1/2)\rho_0\, \mathrm{Re}(A_u A_w^\star)$ is also a function of z.

As shown by Dosser and Sutherland (2011) through manipulation of (3), the wave-induced mean flow of a quasi-monochromatic wave packet is related directly to the momentum flux per unit mass by

$$U = \langle uw\rangle / c_{gz}. \tag{6}$$

This expression is analogous to the relationship between mean energy $\langle E\rangle$ and mean vertical energy flux $\langle F_E\rangle = c_{gz}\langle E\rangle$. Using the polarization relations for anelastic waves (see section 2b and Table 1), we may write U explicitly in terms of the amplitude envelope A_ξ of the vertical displacement field:

$$U = -\frac{1}{2}\frac{1}{c_{gz}}\frac{m\omega^2}{k}\lvert A_\xi\rvert^2 e^{z/H} = \frac{1}{2} NK \lvert A_\xi\rvert^2 e^{z/H}, \tag{7}$$

in which $K = (k^2 + m^2 + 1/4H^2)^{1/2}$. The same result is arrived at by using the polarization relations to compute $-\langle \xi\zeta\rangle$, as in (1).

If a wave packet is initialized with small amplitude and is vertically localized about some arbitrary vertical level, which we take here to be $z = 0$, then (7) shows that the wave-induced mean flow grows exponentially with height as the waves propagate upward. Eventually this transient flow will become so large that it will Doppler-shift the waves, thus changing their structure and consequent evolution. It is this feedback that primarily controls the weakly nonlinear evolution of the waves as they grow to large amplitude.

b. Equations of motion and linear theory

In developing a weakly nonlinear theory for anelastic internal wave packets, we begin by considering the fully nonlinear equations for an inviscid, ideal, anelastic gas (Ogura and Phillips 1962; Lipps and Hemler 1982) that includes an average horizontal flow U:

$$\frac{D\mathbf{u}_T}{Dt} = -\nabla\frac{p}{\overline{\rho}} + \frac{g}{\overline{\theta}}\theta\mathbf{z}, \tag{8}$$

$$\nabla\cdot(\overline{\rho}\mathbf{u}_T) = 0, \tag{9}$$

$$\frac{D\theta_T}{Dt} = 0. \tag{10}$$

In (8) and (10), the material derivative is $D/Dt = \partial_t + \mathbf{u}_T\cdot\nabla$, with $\nabla \equiv (\partial_x, \partial_z)$. The T subscripts denote the total value of a field. Explicitly, the total pressure, density, and potential temperature are respectively decomposed into background and fluctuation components as $P_T = \overline{p}(z) + p(\mathbf{x}, t)$, $\rho_T = \overline{\rho}(z) + \rho(\mathbf{x}, t)$, and $\theta_T = \overline{\theta}(z) + \theta(\mathbf{x}, t)$. Likewise the total velocity is written in terms of the horizontally averaged horizontal flow U and the fluctuation velocity $\mathbf{u} = (u, w)$ by $\mathbf{u}_T \equiv (U + u, w)$. If we assume the background flow is stationary in the absence of waves, then $U = U(z, t)$ is nothing but the wave-induced mean flow given by (6) and (7); it is the transient wind, analogous to the Stokes drift for surface waves, resulting from the presence of the waves themselves.

The background potential temperature is given in terms of the background temperature $\overline{T}$ and pressure $\overline{p}$ by

$$\overline{\theta} = \overline{T}(\overline{p}/P_0)^{-\kappa}, \tag{11}$$

in which P_0 is a reference pressure and $\kappa \simeq 2/7$. In a isothermal atmosphere for which $\overline{T} = T_0$, the background density and potential temperature change exponentially with height with $\overline{\rho}$ given by (4), $\overline{p} = P_0\exp(-z/H)$, and

$$\overline{\theta} = T_0 e^{z/H_\theta}. \tag{12}$$

In terms of temperature the density scale height is $H = RT_0/g$, in which R is the gas constant for air and g is the acceleration of gravity. Here we assume that $H_\theta = H/\kappa$ is sufficiently larger than H that adopting the anelastic approximation is reasonable (Klein 2009). By assuming an isothermal atmosphere, the corresponding stratification is uniform in that the squared buoyancy frequency

$$N^2 = \frac{g}{\overline{\theta}}\frac{d\overline{\theta}}{dz} = \frac{g}{H_\theta} \tag{13}$$

is constant with height.

The evolution of small-amplitude doubly periodic waves is straightforwardly found by linearizing the above equations (which involves setting U, an order amplitude-squared quantity, to zero). Thus we arrive at the dispersion relation

$$\omega^2 = N^2\frac{k^2}{k^2 + m^2 + \dfrac{1}{4H^2}}. \tag{14}$$

The structure of the waves is prescribed through the polarization relations, which interrelate the complex-valued amplitudes of various fields. In what follows, it is convenient to represent each in terms of the mass streamfunction ψ, which, using (9), is implicitly defined so that

$$u = -\frac{1}{\overline{\rho}}\frac{\partial\psi}{\partial z} \quad \text{and} \quad w = \frac{1}{\overline{\rho}}\frac{\partial\psi}{\partial x}. \tag{15}$$

For periodic waves,

$$\begin{aligned}\psi &= \mathrm{Re}\{\rho_0 A_{\psi 0}\exp[\imath(kx + mz - \omega t)]e^{-z/2H}\}\\ &= \rho_0 A_{\psi 0}\cos(kx + mz - \omega t)e^{-z/2H}.\end{aligned} \tag{16}$$

In the bottom expression we have arbitrarily set the phase of the wave so that $A_{\psi 0} = |A_{\psi 0}|$ is real-valued, representing the magnitude of the mass streamfunction at $z = 0$.

Some fields grow and others decay exponentially with height, as indicated in the top portion of Table 1. The left column shows the exponential dependence on z of the velocity, vorticity, vertical displacement, and other fields. The right column relates the (complex valued) amplitude of each field at $z = 0$ to the mass streamfunction amplitude at $z = 0$. For reference, Table 1 also lists expressions for the dispersion relation and its m derivatives and it gives an explicit formula for the wave-induced mean flow in terms of the mass streamfunction and the vertical displacement amplitudes.

To describe a horizontally periodic, vertically localized, quasi-monochromatic wave packet at time $t = 0$, it is sufficient to replace the constant amplitude $A_{\psi 0}$ with the amplitude envelope $A_\psi(z, t = 0) = A_{\psi 0}f(z)$ in which $\max f = 1$. Likewise this substitution gives formulas for

the initial amplitude envelope of the other fields. Next we develop a theory that predicts how the amplitude envelopes change in time if the waves are small and moderately large amplitude.

c. Weakly nonlinear theory

The first step in deriving a weakly nonlinear equation describing the evolution of small- and moderately large-amplitude anelastic waves is to manipulate the fully nonlinear equations of motion to a reduced set of coupled equations. Taking the curl of the momentum equations gives the vorticity equation

$$\partial t\zeta + \frac{g}{\theta}\partial_x\theta = -\mathbf{u}\cdot\nabla\zeta - \frac{1}{H}w\zeta - U\partial_x\zeta - U_{zt} - wU_{zz} - \frac{1}{H}U_z w, \tag{17}$$

in which the subscripts denote partial derivatives and

$$\zeta = \partial_z u - \partial_x w = -\frac{1}{\overline{\rho}}\left(\nabla^2\psi + \frac{1}{H}\frac{\partial\psi}{\partial z}\right) \tag{18}$$

is the spanwise component of vorticity.

Equation (10) is also rewritten by putting only those terms that are linear in fluctuation quantities on the left-hand side of the equation:

$$\partial_t\theta + w\overline{\theta}' = -\mathbf{u}\cdot\nabla\theta - U\partial_x\theta. \tag{19}$$

Together with (15) and (18), (17) and (19) form two coupled equations in ψ and θ, in which it is understood that the wave-induced mean flow U is itself quadratically related to these quantities. The coupled equations can be combined using linear operations to eliminate θ from the left-hand sides of (17) and (19). Abstractly, the result may be written

$$L\psi = N_2(\psi,\theta) + N_U(U;\psi,\theta), \tag{20}$$

in which $L \equiv \partial_{zz}\partial_{tt} + (1/H)\partial_{ztt} + \partial_{xx}N^2$ is a linear differential operator, N_2 involves quadratic products of ψ and/or θ and their derivatives, and N_U involves U and its derivatives and quadratic products of U and its derivatives with ψ or θ and their derivatives.

The next step is to write ψ in the form of a horizontally periodic, vertically confined wave packet in which the maximum initial amplitude $A_{\psi 0} = |-(N/K)A_{\xi 0}|$ and the vertical extent σ are represented in terms of the real-valued nondimensional parameters $\alpha \equiv k|A_{\xi 0}|$ and $\epsilon \equiv (k\sigma)^{-1}$, respectively. Explicitly, we write

$$\psi(x,z,t) = \mathrm{Re}[\rho_0\alpha A(Z,T)e^{\imath(kx+mz-\omega t)}e^{-z/2H}], \tag{21}$$

in which $Z \equiv \epsilon z$ and $T \equiv \epsilon t$. It follows from the polarization relations (see Table 1) that we can write $U \equiv \alpha^2 V(Z,T)$, in which $V = (K/2N)|A|^2 e^{z/H}$ does not depend upon the wave packet's initial amplitude.

These expressions are substituted into (20) and terms involving $e^{\imath kx}$ are then extracted from both sides of the equation. This operation has the result of neglecting the quadratic nonlinear terms denoted by N_2 in (20), consistent with the assumption that the initial weakly nonlinear behavior is governed solely by interactions between the wave packet and the mean flow it induces. The z and t derivatives in (20) are rewritten in terms of Z and T derivatives acting on A through $\partial_z \to \epsilon\partial z + \imath\gamma$ and $\partial_t \to \epsilon\partial_T - \imath\omega$, in which $\gamma = m + l/2H$.

Next we form a regular perturbation expansion of A,

$$A = A_0 + \alpha A_1 + \alpha^2 A_2 + \cdots, \tag{22}$$

with a corresponding expansion of $V = V_0 + \alpha V_1 + \cdots$, and we suppose that dispersion and nonlinearity are balanced so that $\epsilon \sim \alpha \ll 1$.

From the resulting equation involving $A_0, A_1, \ldots$, we derive a sequence of equations by extracting terms in successive orders of α. The $O(\alpha)$ equation retrieves the dispersion relation (14). Making use of the dispersion relation, the $O(\alpha^2)$ equation describes the vertical advection of the wave packet at the group velocity c_{gz}:

$$\partial_T A_0 + c_{gz}\partial_Z A_0 = 0. \tag{23}$$

The next order introduces the leading-order nonlinear term U_{ztt} as well as the leading-order linear dispersion term. Explicitly, in terms of the scaled functions, we get

$$\partial_T A_1 + c_{gz}\partial_Z A_1 = \imath\frac{1}{2}\omega_{mm}\partial_{ZZ}A_0 - \imath k V_0 A_0. \tag{24}$$

It is a useful check on the algebra that the linear dispersion term can be re-expressed into the expected form involving two derivatives of the frequency with respect to the vertical wavenumber. Also as expected, the nonlinear term expresses the Doppler-shifting of the waves by the wave-induced mean flow.

In what follows we show that the next-order equation is necessary to explain the observed symmetry breaking in the evolution of moderately large-amplitude waves. This equation is

$$\partial_T A_2 + c_{gz}\partial_Z A_2 = \imath\frac{1}{2}\omega_{mm}\partial_{ZZ}A_1 + \frac{1}{6}\omega_{mmm}\partial_{ZZZ}A_0 - \imath k(V_0 A_1 + V_1 A_0) + \frac{k}{2KH}(3mH - \imath)(\partial_Z V_0)A_0. \tag{25}$$

Finally, we combine these equations by adding (23) to α times (24) to α^2 times (25), using (22) to recast the result into an equation for A and U and then re-expressing the derivatives in terms of the fast variables z and t. Thus we arrive at the weakly nonlinear equation for the evolution of the mass streamfunction amplitude envelope $A(z, t)$:

$$A_t + c_{gz}A_z = \imath\frac{1}{2}\omega_{mm}A_{zz} + \frac{1}{6}\omega_{mmm}A_{zzz} - \imath kUA + \frac{\omega^2}{2N^2kH}(3mH - \imath)U_zA. \quad (26)$$

Here the nonlinear terms involve the wave-induced mean flow, given in terms of A by

$$U = \frac{1}{2}\frac{K^3}{N}|A|^2e^{z/H}. \quad (27)$$

The coefficients of the linear dispersion terms on the right-hand side of (26) are given in terms of k and $K = (k^2 + m^2 + 1/4H^2)^{1/2}$ in Table 1. Table 2 lists explicit values of these coefficients for three vertical wavenumbers, which are examined in detail here.

From A, we may determine the evolution of more intuitive quantities such as the vertical displacement field:

$$\xi = \mathrm{Re}[A_\xi e^{\imath(kx+mz-\omega t)}e^{z/2H}],$$
$$A_\xi(z,t) = -\frac{K}{N}A(z,t). \quad (28)$$

Neglecting the second and fourth terms on the right-hand side of (26) and using (27), we see that the result is the nonlinear Schrödinger equation, (2), cast in a stationary frame rather than in a frame moving with the group velocity, as is usual. With the inclusion of only the first three terms on the right-hand side of (26), in the limit $H \to \infty$ the equation becomes that for Boussinesq waves (Sutherland 2006b). If furthermore we neglect the third-order term, we are left with a special case of the formula derived by Akylas and Tabaei (2005).

It is remarkable that (26) is similar to the corresponding weakly nonlinear equation found by Dosser and Sutherland (2011) for non-Boussinesq internal waves in a liquid. In the fully nonlinear equations used as a starting point in that study, ρ (not θ) served as a thermodynamic variable, the assumption of incompressibility changed the continuity equation, and the pressure gradient term in the momentum equations was different. Nonetheless, the only significant difference in the weakly nonlinear equation arises in the fourth term: the coefficient $(3mH - \imath)$ in (26) is replaced by $(mH + \imath)$ in Dosser and Sutherland (2011).

Equation (26) describes both the linear dynamics associated with the translation and dispersion of a small-amplitude wave packet [in which case the third and fourth terms on the right-hand side of (26) have negligible influence] and the consequent weakly nonlinear dynamics, which become evident when the wave packet has propagated vertically above heights where U, given by (27), is so large that the effect of Doppler-shifting by the wave-induced mean flow is no longer negligible. We estimate the amplitude at which weakly nonlinear effects become nonnegligible by considering the ratio of the leading-order nonlinear term with the linear term describing the vertical advection of the wave packet at the vertical group velocity. When the ratio of the magnitude of these terms is Δ, the magnitude of the wave-induced mean flow is $U = \Delta\epsilon c_{gz}$, in which as above $\epsilon = 1/(k\sigma)$ measures the vertical extent of the wave packet. Below we show that nonlinear effects become significant if $U > \Delta\epsilon c_{gz}$ with $\Delta \simeq 1$. In terms of the maximum vertical displacement amplitude, this condition is met when

$$\|\xi\| \sim \frac{1}{K^2}\sqrt{\frac{2\Delta|m|}{\sigma}}. \quad (29)$$

TABLE 2. The frequency ω, vertical group velocity $c_{gz} = \omega_m$, and higher m derivatives of ω computed for three values of m/k and with $Hk = 10$.

m/k	ω/N	$c_{gz}\frac{k}{N}$	$\omega_{mm}\frac{k^2}{N}$	$\omega_{mmm}\frac{k^3}{N}$
−0.4	0.93	0.32	−0.470	−1.91
−0.7	0.82	0.38	−0.008	−1.05
−1.4	0.58	0.27	0.193	0.09

d. Solution of the NLS equation

As an illustration of the evolution of a weakly nonlinear wave packet, Fig. 1 shows the evolution of a nonhydrostatic wave packet at three different times. The initially horizontally periodic, vertically Gaussian wave packet is prescribed so that the vertical displacement field is

$$\xi(x, z, 0) = A_{\xi 0}e^{-z^2/2\sigma^2}\cos(kx + mz)e^{z/2H}, \quad (30)$$

in which $m = -0.4k$, $kA_{\xi 0} = 0.05$, $k\sigma = 10$, and $kH = 10$. The relative vertical wavenumber and wave packet extent have been chosen so that the results may be compared with the weakly and fully nonlinear simulations of moderately large-amplitude Boussinesq wave packets (Sutherland 2006b). Here the density scale height is finite so that wave packets starting with small amplitude grow as they propagate upward until nonlinear effects become significant.

In all simulations, the horizontal wavenumber k is fixed and the buoyancy frequency N is constant. For convenience we use these values as respective measures of length and time scales. Thus, for example, we represent the frequency and vertical group velocity of the wave

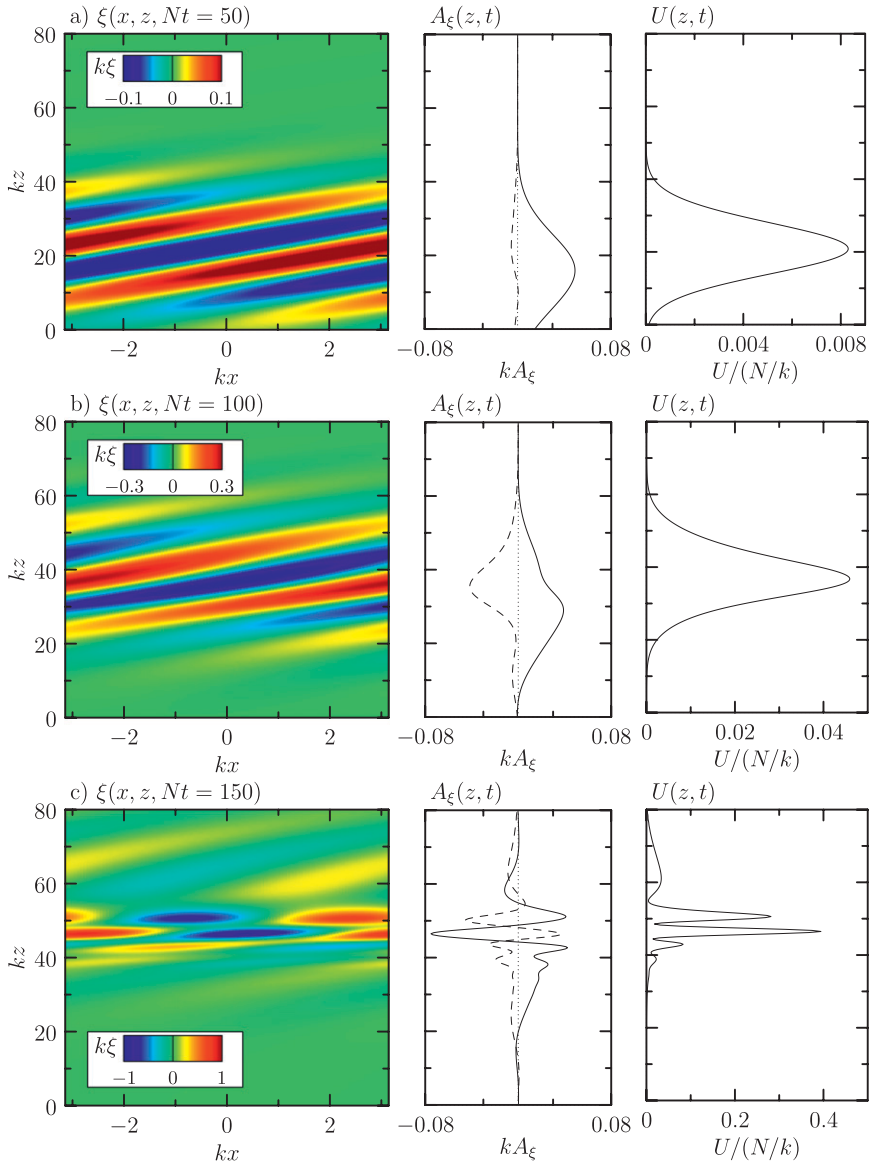

FIG. 1. Evolution of a weakly nonlinear wave packet with $m = -0.4k$ at times (a) $t = 50N^{-1}$, (b) $100N^{-1}$, and (c) $150N^{-1}$. The Gaussian wave packet is centered initially about $z = 0$ with width $\sigma = 10k^{-1}$ and amplitude $A_{\xi 0} = 0.05k^{-1}$. It propagates upward through an anelastic gas with density scale height $H = 10k^{-1}$. (left) Snapshots of the vertical displacement field; (middle) real (solid) and imaginary (dashed) parts of its amplitude envelope $A_\xi(z,t)$; (right) the corresponding wave-induced mean flow U.

packet with $m = -0.4k$ and $H = 10k^{-1}$ by $\omega \simeq 0.81N$ and $c_{gz} \simeq 0.32N/k$, respectively.

In practice, from the polarization relations, (30) is used to define the mass streamfunction so that its initial amplitude envelope is

$$A(z,0) = -(N/K)A_{\xi 0}e^{-z^2/2\sigma^2}. \tag{31}$$

This is used as the initial condition in the solution of (26). The equation is solved by computing $\partial_t A$ from the spatial derivatives on the left- and right-hand sides of (26). This time derivative is used to advance A by a small increment in time, and the procedure then repeats. For the results illustrated in Fig. 1, the wave packet was embedded in a domain ranging over $-150 \le kz \le 150$ with a resolution of $\Delta z \simeq 0.3k^{-1}$ and the field was advanced in time by steps of $0.0001N^{-1}$.

At time $t = 50N^{-1}$, A_ξ is predominantly real-valued with little change from its initial Gaussian shape. As expected for a small-amplitude wave packet, the envelope

has translated upward at the group velocity, its center being located at $kz = 16.0$. Although the peak value of A_ξ is $0.0494k^{-1}$, moderately smaller than the initial amplitude, the actual maximum vertical displacement is much larger as a consequence of anelastic growth over 1.6 density scale heights. The peak value of ξ is $0.124k^{-1}$, occurring at $kz = 20.9$, larger than the peak of A_ξ by the exponential factor $e^{z/2H}$. The wave-induced mean flow likewise exhibits a peak about $kz = 20.9$. The behavior up until this time differs little from linear theory, consistent with the fact that the peak wave-induced mean flow is much smaller than $\epsilon c_{gz} \simeq 0.032N/k$.

The effects of weak nonlinearity become apparent at time $t = 100N^{-1}$, as shown in Fig. 1b. The maximum value of the wave-induced mean flow at this time is comparable to ϵc_{gz}, sufficiently large that it nonnegligibly Doppler-shifts the wave packet, more so above its center. The Doppler shifting is apparent in the plot for A_ξ, which shows a substantial change in the imaginary part. This results in a phase shift of the waves near the center of the wave packet. The corresponding color contours of ξ show that the lines of constant phase tilt more toward the vertical near the center of the wave packet than at the leading and trailing edges.

The interaction between the waves and wave-induced mean flow continues to distort the wave packet, dramatically changing its structure at later times. At $t = 150N^{-1}$, the differential changes with height in the phase of the wave packet have altered its structure so much that it is questionably considered to be quasi-monochromatic. The maximum vertical displacement is as large as $k_\xi = 0.85$, which gives some indication that the wave packet is close to overturning.

The evolution of strongly and weakly nonhydrostatic internal wave packets is shown in Fig. 2 by way of time series of the wave-induced mean flow. The circumstance discussed above in which $m = -0.4k$ is shown in Figs. 2a and 2d. In Fig. 2a its initial exponential growth with height is evident as it moves vertically at the group velocity, c_{gz}. In Fig. 2d the result of the same simulation is shown but the wave-induced mean flow is multiplied by $e^{-z/H}$ so as to remove the anelastic growth predicted by linear theory. The resulting field is then plotted in a frame of reference, $Z = z - c_{gz}t$, moving with the vertical group velocity. In the absence of weakly nonlinear effects, the resulting plot would appear as a horizontal band across the panel, with moderate broadening due to linear dispersion. Plotted as such, the onset of weakly nonlinear dynamics becomes evident around time $t = 100N^{-1}$. Shortly thereafter the wave packet narrows and peaks. This is followed by a deceleration of the wave packet as successive peaks develop toward its trailing edge.

The development of the first peak is a consequence of modulational instability. Mathematically it results from the leading-order nonlinear (Doppler-shifting) term of the nonlinear Schrödinger equation. The next higher-order linear and nonlinear terms are responsible for the symmetry breaking leading to the deceleration of the wave packet. Without these terms the wave packet would undergo the so-called Fermi–Pasta–Ulam recurrence in which the wave packet repeatedly narrows and broadens but with no change in its group velocity.

From (26) and noting that kU is positive, the modulational stability of the wave packet (Whitham 1974) depends on the sign of ω_{mm}. Explicitly, wave packets are modulationally unstable if

$$|m/k| < 2^{-1/2}\left[1 + \frac{1}{(2kH)^2}\right]^{1/2} \tag{32}$$

and are modulationally stable otherwise. If the density scale height is relatively large, the critical vertical wavenumber is $|m| = 2^{-1/2}|k| \simeq 0.71|k|$, as is the case for Boussinesq waves. For relatively large horizontal wavelength waves ($kH \ll 1$), the critical vertical wavenumber is $|m| = 8^{-1/2}/H \simeq 0.35/H$. Thus, long waves are modulationally unstable if their vertical wavelength is longer than approximately $18H \gg 100$ km, using typical density scale heights of the atmosphere. All of this is to say that the most energetic internal atmospheric waves are modulationally stable.

An example of a modulationally stable wave packet is shown in Figs. 2c and 2f. In this case the background and the initial wave packet have the same structure as the case described above except that now the vertical wavenumber is $m = -1.4k$. As expected for a modulationally stable wave packet, when nonlinear effects become nonnegligible the wave packet broadens and its peak (multiplied by $e^{-z/H}$) decreases much more quickly than would occur due to linear dispersion alone. Looking at Fig. 2f these weakly nonlinear effects begin to become important around time $t = 75N^{-1}$. At much later times (around $t = 75N^{-1}$) the leading edge of the wave packet begins to break up so that the wave-induced mean flow becomes a series of jets.

The marginally unstable case is shown in Figs. 2b and 2e, for which $m = -0.7k$. Here the wave packet exhibits features of modulational stability and instability. Near time $t = 75N^{-1}$, the wave packet broadens as the peak (multiplied by $e^{-z/H}$) decreases. But starting around time $t = 120N^{-1}$ the wave packet narrows and peaks near the leading edge of the wave packet. Successive peaks then develop from the leading to trailing edge of the wave packet.

The dynamics of modulationally stable and unstable wave packets demonstrate that anelastic internal wave

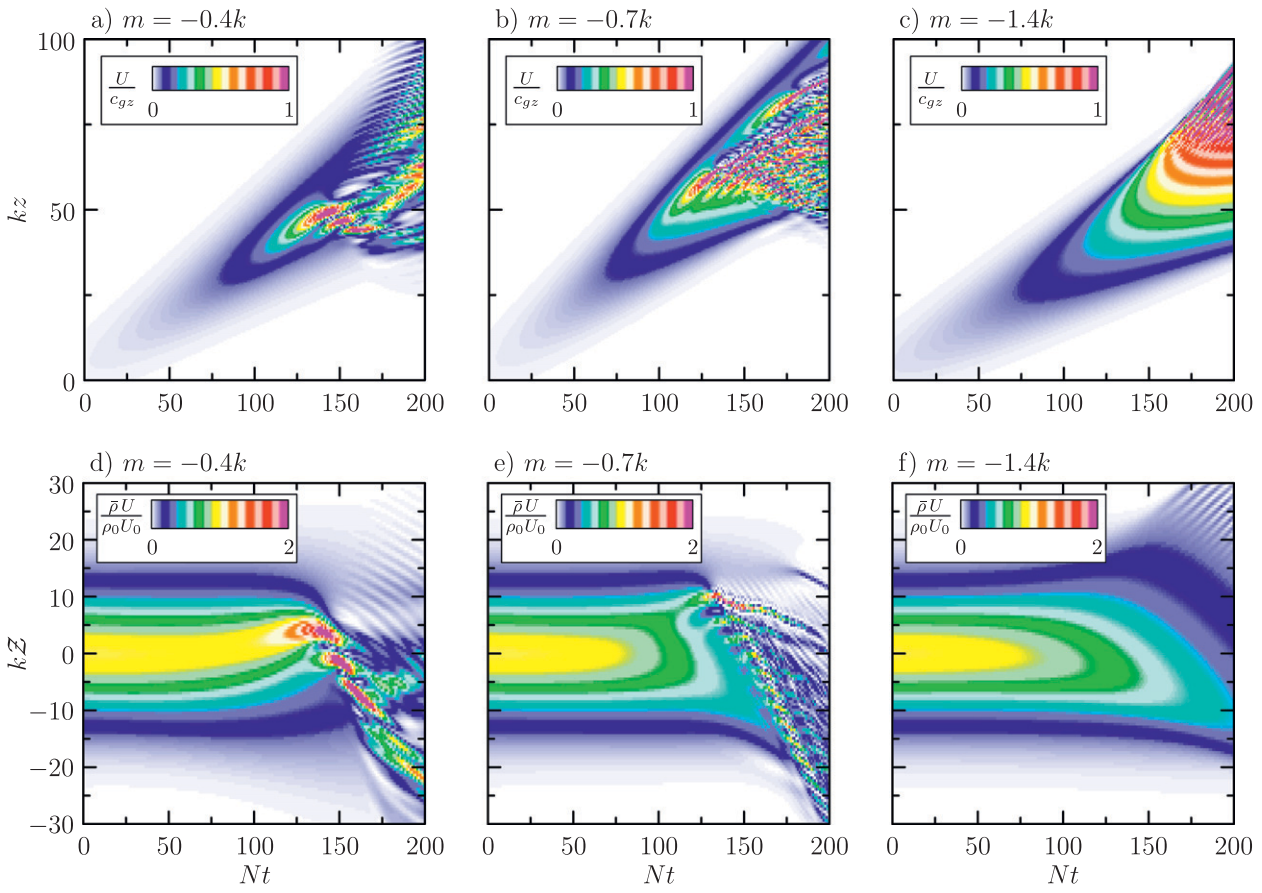

FIG. 2. Time series showing the evolution of the wave-induced mean flow $U(z, t)$ associated with wave packets having vertical wavenumber m equal to (a),(d) $-0.4k$, (b),(e) $-0.7k$, and (c),(f) $-1.4k$. In each case, the Gaussian wave packets are centered initially about $z = 0$ with width $\sigma = 10k^{-1}$ and amplitude $A_{\xi 0} = 0.05k^{-1}$, and they propagate upward through an anelastic gas with density scale height $H = 10k^{-1}$. In (a)–(c), the indicated color scale shows values of U normalized by the vertical group velocity c_{gz}. In the corresponding plots in (d)–(f), the wave-induced mean flow is multiplied by the background density profile $\overline{\rho}/\rho_0 = \exp(-z/H)$ and is further normalized by the peak initial value of the wave-induced mean flow $U_0 = NK|A_{\xi 0}|^2/2$. The result is shifted into a frame of reference moving with the vertical group velocity $z \rightarrow \mathrm{Z} = z \rightarrow c_{gz}t$.

packets evolve in a qualitatively different manner than predicted by linear theory. In particular, because modulationally unstable wave packets narrow and their peak value initially grows faster than exponentially, we expect such waves should overturn and begin to break below the height predicted by linear theory. Conversely, modulationally stable wave packets should propagate above the breaking level predicted by linear theory before they grow to such an amplitude that they overturn.

In the next section we investigate these claims by performing fully nonlinear simulations of anelastic internal wave packets.

3. Fully nonlinear evolution

Here we describe the method used to solve the fully nonlinear anelastic equations, we compare the results with the solutions of the weakly nonlinear equation described in the last section, and we go on to diagnose at what heights anelastic internal wave packets become overturning.

a. Numerical simulation method

The fully nonlinear 2D anelastic code solves the coupled equations for spanwise vorticity ξ and potential temperature θ in a horizontally periodic domain with free-slip upper and lower boundary conditions. Without explicitly separating fluctuation and mean-flow contributions, as in (17), and including dissipation, the vorticity equation is

$$\frac{D\zeta}{Dt} = -\frac{1}{H}w\zeta - \frac{g}{\bar{\theta}}\frac{\partial\theta}{\partial x} + C_\zeta\nabla^2\zeta. \tag{33}$$

The dissipation term $C_\zeta\nabla^2\zeta$ has the effect of including viscosity except that the coefficient C_ζ is taken to be

larger than the kinematic viscosity of air. The term is introduced to keep the code numerically stable through the damping of small-scale noise. However, the coefficient is still taken to be sufficiently small that dissipation negligibly affects the dynamics. Typically we take $C_\zeta = 10^{-4}N/k^2$. No significant quantitative changes in the results were found by doubling C_ζ.

Also for the purposes of numerical stability, the internal energy equation [(10)] is modified by the addition of a diffusion term:

$$\frac{D\theta}{Dt} = -w\frac{d\bar{\theta}}{dz} + C_\theta \nabla^2\theta, \tag{34}$$

in which we set $C_\theta = C_\zeta$.

For given ζ, (18) is inverted to find the mass streamfunction ψ and this is used to find the velocity fields through (15). To perform the inversion and compute derivatives it is convenient to work with the fields being vertically discretized on an evenly spaced grid and being Fourier decomposed in the horizontal. This methodology is analogous to that used in the solution of the 2D Boussinesq equations (Sutherland and Peltier 1994).

The vertical extent of the domain is set to be large enough that the waves are of negligibly small amplitude at the boundaries over the duration of each simulation. In typical runs, the domain ranges between $z = -150k^{-1}$ and $150k^{-1}$ with a resolution of $\Delta z = 0.3k^{-1}$. In the horizontal, wavenumbers between 0 and $8k$ are resolved. Doubling the resolution was found to have no significant quantitative effect on the wave dynamics.

The equations are advanced in time using the ''leapfrog'' method, with an Euler backstep taken every 20 time steps. The time step typically used in simulations was $\Delta t = 0.025N^{-1}$.

In the simulations reported here we solve the initial value problem in which a horizontally periodic, vertically Gaussian quasi-monochromatic wave packet is prescribed in the middle of the domain at $t = 0$. Explicitly, the simulations are set up so that the initial vertical displacement field is given by (30). Using the polarization relations, the code approximates the initial mass streamfunction as

$$\psi(x, z, 0) = \rho_0 A_{\psi 0} e^{-z^2/2\sigma^2} \cos(kx + mz) e^{-z/2H}, \tag{35}$$

in which mass is scaled so that $\rho_0 = 1$ and $A_{\psi 0} = -(\omega/k)A_{\xi 0}$, with ω set through the dispersion relation (14). From this, the initial velocity and vorticity fields are computed. Likewise the code uses the polarization relations to initialize the fluctuation potential temperature (see Table 1).

Another step in the initialization of the code is to use (1) to define the initial wave-induced mean flow $U(z, 0)$ from the initial vorticity and vertical displacement fields. Its z derivative U_z is then added to the horizontal wavenumber-zero component of the vorticity field. The step of including the initial wave-induced mean flow is physically realistic but practically unnecessary in simulations initialized with a small-amplitude wave packet. If the simulation started with zero background flow (hence zero background vorticity), a short time after the simulation began an unchanging jet would emerge that flows in the negative direction centered about $z = 0$ (the position from which the wave packet originated). Concurrently a positive-flowing jet would develop at the level of the wave packet, its peak moving upward concurrent with the wave packet's upward translation. The negative jet near $z = 0$ is given exactly by $-U(z, 0)$, this being the deficit of flow arising because the wave-induced mean flow was not included at the outset. Because momentum is conserved in the domain and the initial mean momentum is zero, the vertically integrated positive momentum associated with the upward-translating jet is equal and opposite to the integrated negative momentum associated with the jet near $z = 0$. All of this is to say that the wave-induced mean flow develops around the wave packet whether or not it is explicitly prescribed initially.

b. *Fully nonlinear simulation results*

For the purposes of comparing the fully nonlinear simulation results with the weakly nonlinear results of the last section as well as with the Boussinesq simulations of Sutherland (2006b), we first report on simulations in which $A_{\xi 0} = 0.05k^{-1}$ is the maximum initial vertical displacement, $\sigma = 10k^{-1}$ is the wave packet width, and $H = 10k^{-1}$ is the density scale height. We first focus on the evolution of a wave packet with $m = -0.4k$ and then examine cases with $m = -0.7k$ and $-1.4k$. In the discussion on wave overturning that follows, a wider range of parameters are explored.

If we take $N = 0.01s^{-1}$ as a characteristic value of the buoyancy frequency in the stratosphere, then it follows from (13) that the corresponding density scale height for the isothermal gas is $H = kg/N^2 \simeq 28$ km. Therefore, corresponding to $kH = 10$, the horizontal wavelength is approximately 18 km ($k = 0.36$ km^{-1}) and, corresponding to $kA_{\xi 0} = 0.05$, the initial maximum vertical displacement amplitude is 140 m.

The evolution of the wave packet with $m = -0.4k$ is shown in Fig. 3. The panels should be compared with the vertical displacement fields predicted by weakly nonlinear theory, which are shown in the left column of Fig. 1. The structure and amplitude of the wave packet at times $t = 50N^{-1}$ and $100N^{-1}$ are nearly the same in both fully and weakly nonlinear simulations. For example, the peak vertical displacement at $t = 100N^{-1}$ is $0.283k^{-1}$ in the

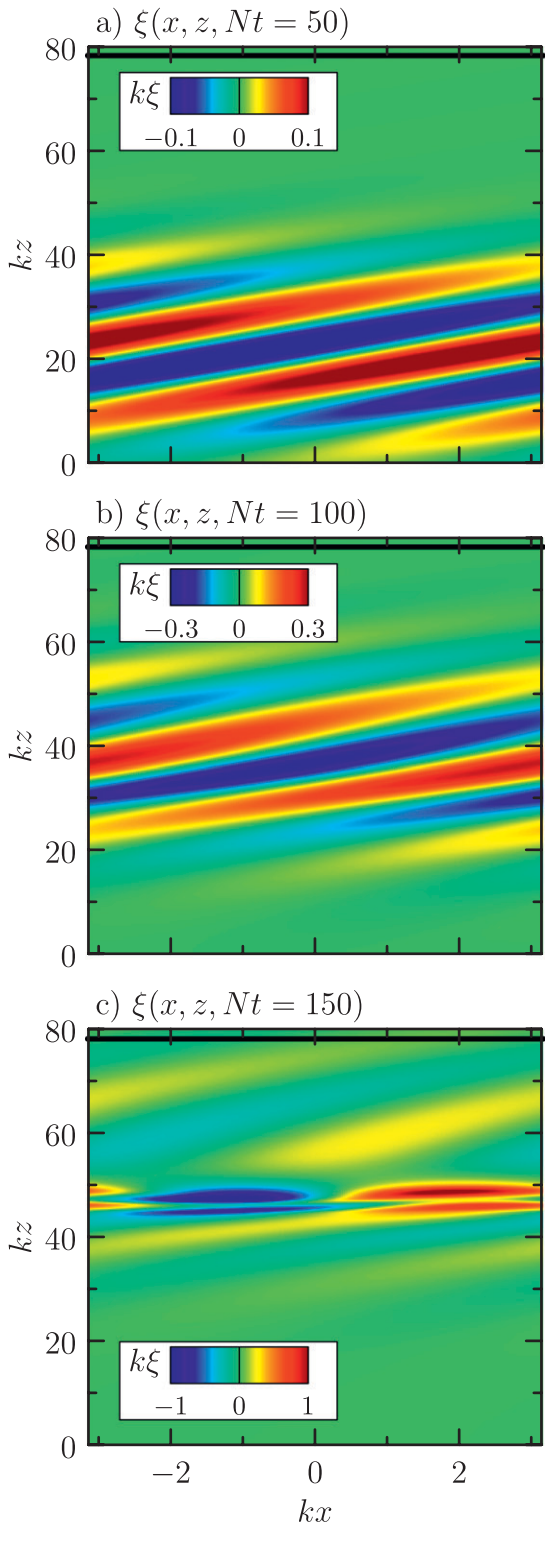

FIG. 3. Solution of the fully nonlinear anelastic equations showing the evolution of the (nondimensional) vertical displacement field $k\xi(x, z, t)$ at (nondimensional) times Nt = (a) 50, (b) 100, and (c) 150. The initial wave packet with $m = -0.4k$ is a Gaussian centered about $z = 0$ with $\sigma = 10k^{-1}$ and amplitude $kA_{\xi 0} = 0.05$. The density scale height is $10k^{-1}$. The horizontal black line near the top of each plot indicates the breaking level predicted by linear theory.

fully nonlinear simulation (Fig. 3b), whereas it is $0.292k^{-1}$ in the weakly nonlinear case (Fig. 1b). The similarity between simulations during the linear and early weakly nonlinear times of the wave packet's evolution demonstrates that the diffusion terms introduced in (33) and (34) indeed have negligible influence. Furthermore, the similarity of the fully and weakly nonlinear simulations at $t = 100N^{-1}$ corroborates the weakly nonlinear theory hypothesis that the nonlinear dynamics are governed by interactions between waves and the transient mean flow they induce. At least initially, parametric subharmonic instability (Klostermeyer 1982; Lombard and Riley 1996) and other mechanisms that involve the nonlinear transfer of energy to superharmonics have insignificant impact on the evolution of the wave packet.

Even at $t = 150N^{-1}$ when the wave packet has undergone significant distortion as a consequence of nonlinear dynamics, the fully nonlinear wave packet shown in Fig. 3c has qualitatively similar structure to the weakly nonlinear wave packet shown in Fig. 1c. The vertical structure has narrowed significantly and the peak values are comparable: in the weakly nonlinear simulation the peak vertical displacement is $0.85k^{-1}$ occurring at height $z \simeq 46k^{-1}$; in the fully nonlinear simulation the peak of $0.79k^{-1}$ occurs at $z = 46k^{-1}$. In both cases the wave packet has grown to much larger amplitude than predicted by linear theory on the basis of anelastic growth alone. At time $t = 150N^{-1}$ linear theory predicts the wave packet should have translated upward to $z \simeq 48k^{-1}$ where its peak value should be $A_{\xi 0} \exp(z/2H) \simeq 0.55k^{-1}$. Below we show that the increased growth due to modulational instability is so large that the waves are close to overturning at this time although the wave packet is situated well below the predicted overturning height of $z_b = 78k^{-1}$.

As shown in the study of weakly nonlinear wave packets, the amplitude of a modulationally stable wave packet grows less quickly with height than predicted by linear theory. This is confirmed by the fully nonlinear simulation results shown in Fig. 4. Here the amplitude, wave packet width, and density scale height are respectively $A_{\xi 0} = 0.05k^{-1}$, $\sigma = 10k^{-1}$, and $H = 10k^{-1}$, as before, but the vertical wavenumber is $m = -1.4k$. Because of anelastic growth, the wave packet is predicted to grow to overturning amplitudes at $z_b = 53k^{-1}$, reaching this height at time $t \simeq 196N^{-1}$. However, the simulation shows that the wave packet propagates well above this level. At time $t = 150N^{-1}$, the weakly nonlinear effect of modulational stability has reduced the amplitude of the wave packet as it has broadened in vertical extent. The maximum vertical displacement at this time is $0.36k^{-1}$ occurring at $z \simeq 42k^{-1}$. Linear theory predicts the center of the wave packet should have moved upward to $z \simeq 41k^{-1}$ where its peak amplitude should be $A_{\xi 0} \exp(z/2H) \simeq 0.38k^{-1}$. At time $t = 200N^{-1}$

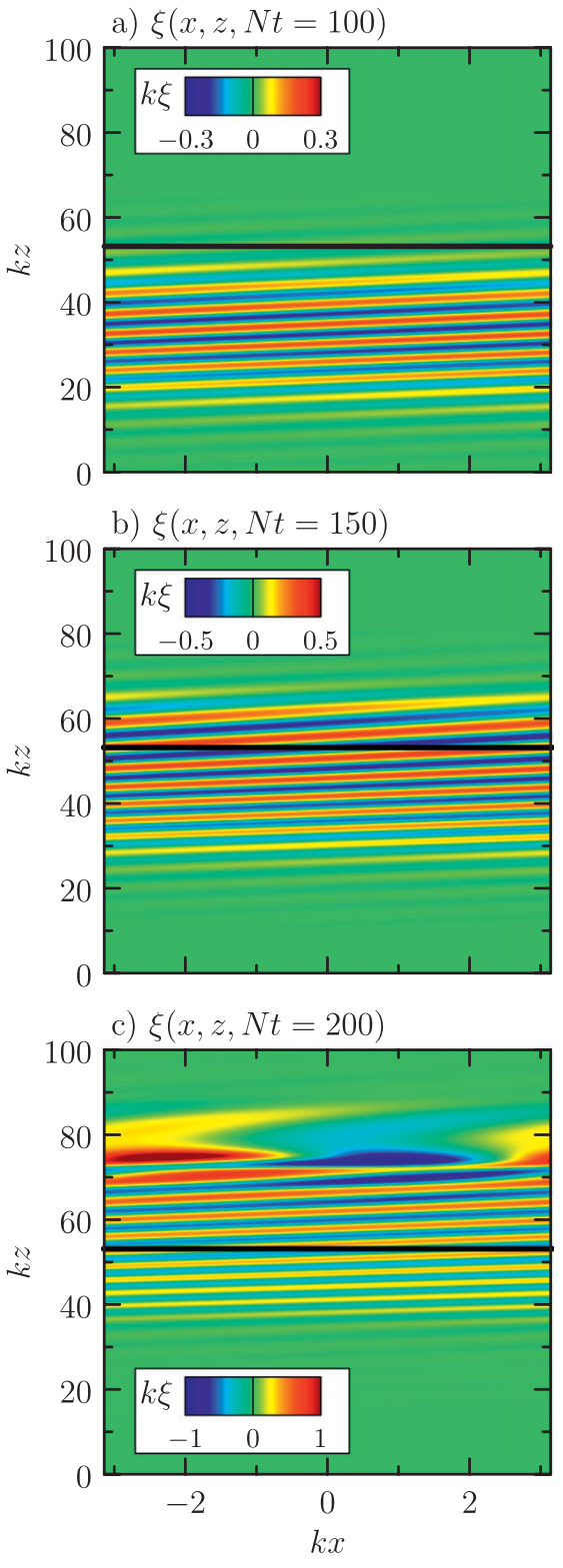

FIG. 4. As in Fig. 3, but showing the evolution of a wave packet with $m = -1.4k$ at times Nt = (a) 100, (b) 150, and (c) 200. The breaking level predicted by linear theory is indicated by the horizontal black line.

the maximum vertical displacement at the predicted breaking level is only $0.44k^{-1}$, 60% the value predicted by linear theory. The maximum vertical displacement of $1.23k^{-1}$ instead occurs at $z \simeq 75k^{-1}$.

The life cycle of modulationally stable and unstable wave packets is illustrated through time series of their wave-induced mean flow, as shown in Fig. 5. These present the results of fully nonlinear simulations in which the initial conditions each set $A_{\xi 0} = 0.05k^{-1}$, $\sigma = 10k^{-1}$, and $H = 10k^{-1}$ but the relative vertical wavenumber is $m = -0.4k$, $-0.7k$, and $-1.4k$. The plots are multiplied by $\exp(-z/H)$ and shifted into a frame of reference translating with the vertical group velocity ($Z = z - c_{gz}t$) so that they can be compared directly with the scaled and shifted time series of the corresponding weakly nonlinear simulations shown in the bottom panels of Fig. 2.

As in the weakly nonlinear simulations, we find that the early evolution of each wave packet obeys linear theory and that weakly nonlinear dynamics develop between $t \approx 70N^{-1}$ and $100N^{-1}$. In comparison with Fig. 2d, Fig. 5a shows that the wave packet narrows and peaks moderately above the center of the wave packet and then successive peaks form toward the trailing edges of the wave packet. In the fully nonlinear simulation, the wave packet first becomes overturning at $t = 158N^{-1}$. This is measured by determining the minimum value of the total squared buoyancy frequency $N_T^2 = N^2 + \Delta N^2$ in which

$$\Delta N^2 \equiv \frac{g}{\overline{\theta}} \frac{\partial \theta}{\partial z}. \tag{36}$$

The waves are overturning where N_T^2 is negative and the resulting growth rate of convective instability is proportional to $|N_T|$ (see the appendix). Just because the waves are overturning does not mean that convection begins. The oscillating motion associated with the waves can restabilize the negatively buoyant fluid if the wave period is sufficiently short compared to the time for convective growth (Sutherland 2001). However, after another 1.5 buoyancy periods ΔN^2 is so much less than N^2 that convection causes energy to cascade efficiently to small scale. At $t = 168N^{-1}$ this process makes the code numerically unstable. Although we could have run the code at higher resolution so as to prevent its instability, such an effort is pointless since the realistic physics of convection cannot be captured by a code restricted to two spatial dimensions. We restrict our study here to waves that evolve to the point of overturning. Simulations performed with higher resolution confirm that the time and location at which overturning first occurs are insensitive to resolution. This result is consistent with that found by Sutherland (2001) for large-amplitude Boussinesq waves.

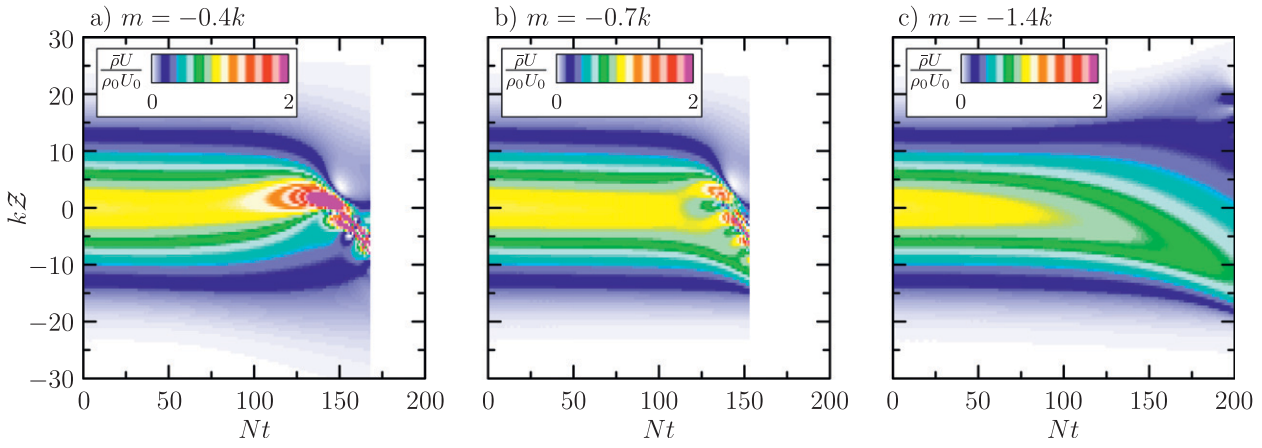

FIG. 5. Time series of the normalized wave-induced mean flow determined from fully nonlinear simulations with $kA_{\xi 0} = 0.05$, $k\sigma = kH = 10$, and vertical wavenumber m equal to (a) $-0.4k$, (b) $-0.7k$, and (c) $-1.4k$. To focus on departures from anelastic growth predicted by linear theory, the wave-induced mean flow is multiplied by the background density profile $\bar{\rho}/\rho_0 = \exp(-z/H)$ and is further normalized by the peak initial value of the wave-induced mean flow $U_0 = NK|A_{\xi 0}|^2/2$. The vertical axis is given in terms of the translating coordinate $\mathcal{Z} = z - c_{gz}t$. In (a) and (b), the field is plotted only until $t = 168N^{-1}$ and $153N^{-1}$, respectively, when overturning renders the simulation numerically unstable.

The fully nonlinear simulation with $m = -0.7k$ (Fig. 5b) likewise behaves similarly to the corresponding weakly nonlinear model (Fig. 2e). The wave packet broadens slightly before narrowing and increasing in relative amplitude. Thus, it first demonstrates features of modulational stability but then rapidly becomes unstable. The waves become overturning at an earlier time in part because the vertical group velocity is fastest for this relative vertical wavenumber and so anelastic growth occurs more quickly.

Finally, in the simulations of the more hydrostatic wave packet with $m = -1.4k$ (Fig. 5c) the decrease in amplitude relative to anelastic growth is apparent just as it was in the weakly nonlinear case (Fig. 2f). The finescale jets that develop after $t = 150N^{-1}$ at the leading edge of the weakly nonlinear wave packet are not apparent in the fully nonlinear simulation. Nonetheless, the latter does show a relative increase in the wave-induced mean flow shortly before the time at which the waves become overturning. The waves first become overturning at time $t = 196N^{-1}$ near $z \simeq 72k^{-1}$ but continue to evolve for another three buoyancy periods until convection efficiently cascades energy to small scales.

c. *Breaking heights*

Clearly nonlinear effects significantly change the time and height at which a wave packet breaks. The case studies above show that the modulationally unstable wave packet overturns well below the level predicted by linear theory and the modulationally stable wave packet propagates well above this level.

Here we quantify this further by examining how the relative breaking height changes with the density scale height and with wave packet width and vertical wavenumber. The conditions used to diagnose wave overturning in the fully nonlinear simulations, as well as the determination of the predicted overturning heights from linear theory, are given in the appendix.

Figure 6 shows the overturning heights for a range of simulations in which the vertical wavenumber and density scale height relative to the horizontal wavenumber are varied. In each plot the vertical axis is normalized by the density scale height. In most simulations the vertical extent of the initial wave packet was taken to be $\sigma = 10k^{-1}$, although breaking heights for wave packets with smaller initial widths are considered in Fig. 6c. Here $|m/k| = 1.4$ is sufficiently large that the wave packet can be considered to be quasi-monochromatic even with $\sigma = 2k^{-1}$.

In all cases the initial maximum vertical displacement amplitude is taken to be $A_{\xi 0} = 0.05k^{-1}$, sufficiently small that weakly nonlinear effects are not significant at time $t = 0$. As an indication of the heights at which large-amplitude effects become important, we use the condition given by (29) to plot the heights z_Δ where

$$z_\Delta/H = 2\ln\left(\frac{1}{A_{\xi 0}K^2}\sqrt{\frac{2\Delta|m|}{\sigma}}\right). \tag{37}$$

This is the height where the leading-order nonlinear term of the nonlinear Schrödinger equation is comparable to the leading-order linear (advective) term such that $U/c_{gz} = \Delta/(k\sigma)$. Values of z_Δ are plotted as the long-dashed lines in Fig. 6 for $\Delta = 1$. This indicates the height at which the wave packet has grown to such amplitude that the weakly nonlinear effects of modulational stability and instability

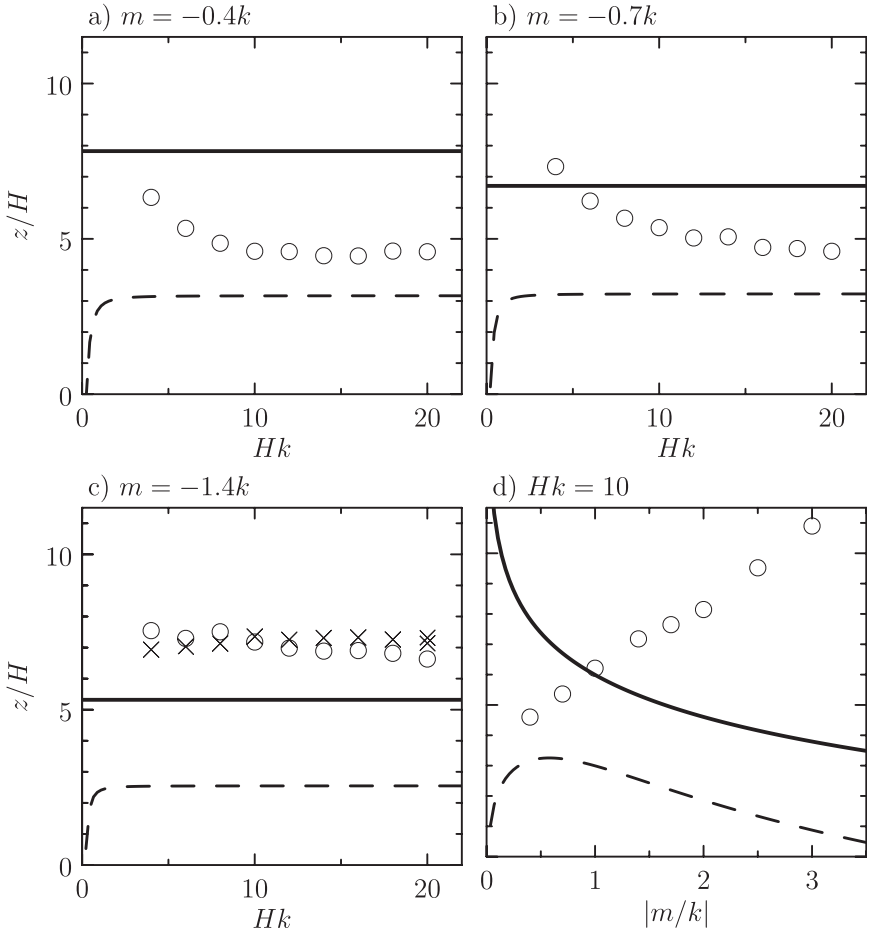

FIG. 6. Height where wave packets first overturn as determined from fully nonlinear simulations with varying Hk and m = (a) $-0.4k$, (b) $-0.7k$ and (c) $-1.4k$, and (d) with varying m and $Hk = 10$. In all cases the initial Gaussian wave packet is centered about $z = 0$ with maximum vertical displacement amplitude $A_{\xi 0} = 0.05k^{-1}$ and with width $\sigma = 10k^{-1}$ (open circles). In (c), overturning levels with $\sigma = 2k^{-1}$ (crosses) are also shown. The breaking height predicted by linear theory is shown by the thick horizontal line in each plot. Also shown is the height given by (37) where weakly nonlinear effects begin to become important as measured by $\Delta = 1$ (long-dashed line).

begin to become significant. The distance between the measured overturning levels and the values of z_Δ provides some indication for the distance over which a large-amplitude wave packet propagates before breaking.

Also for comparison, Fig. 6 indicates where linear theory predicts breaking should occur. Because $A_{\xi 0}k$ is constant the predicted breaking height, given by (A2), is constant for fixed relative vertical wavenumber m/k. This is plotted as the solid lines in Fig. 6.

As expected for modulationally unstable wave packets, strongly nonhydrostatic waves with $m = -0.4k$ overturn well below the height predicted by linear theory (Fig. 6a). For moderate values of k relative to the density scale height H, the breaking level occurs above z_Δ only a quarter of the distance between z_Δ and z_b [the breaking height predicted by (A2)]. This corresponds to a breaking level tens of kilometers below the predicted breaking level in a realistic atmosphere.

Conversely, but as expected for modulationally stable wave packets, the more hydrostatic waves with $m = -1.4k$ overturn well above the height predicted by linear theory (Fig. 6c). For moderate values of Hk, the actual overturning height is about a third more than the distance between z_b and z_Δ or on the order of 10 km. For a fixed value of $k = 10H^{-1}$, Fig. 6d shows that simulated overturning height occurs further above the predicted breaking height for wave packets with larger values of $|m|$.

4. Conclusions

We have derived the nonlinear Schrödinger equation for horizontally periodic anelastic internal waves. Through

comparison of its results with those of fully nonlinear numerical simulations, we have shown that it well captures the weakly nonlinear dynamics of nonrotating waves in uniform stratification with uniform (or zero) ambient wind. The results apply to both hydrostatic and nonhydrostatic internal waves as well as to waves with zero (stationary) or nonzero ground-relative horizontal phase speed. Thus, we have demonstrated that the Doppler shifting of the waves by their wave-induced mean flow (their Stokes drift) dominates the evolution of vertically localized wave packets. Wave–wave interactions leading to parametric subharmonic instability may dominate for plane periodic waves (Klostermeyer 1982; Fritts et al. 1994; Lombard and Riley 1996; Sutherland 2006a) but not wave packets.

Because of modulational instability, weakly and fully nonlinear simulations have shown that wave packets break below the level predicted by linear theory if their frequency is sufficiently close to the buoyancy frequency. In terms of the relative vertical wavenumber, the condition for instability is given by (32). Most relevant to the parameterization of gravity wave drag in general circulation models, we found that the lower-frequency, hence energy-containing, internal waves are modulationally stable. This means that their increase in amplitude due to anelastic growth is retarded and so they break above the level predicted by linear theory. For sufficiently short horizontal wavelength waves ($\lambda_x \lesssim 20H$) the simulated overturning height depends weakly on the wave packet's vertical extent but increases with relative vertical wavenumber $|m/k|$. Using characteristic atmospheric parameters, simulations show that the difference between the predicted and actual overturning levels can be on the order of tens of kilometers.

As an example, if the density scale height is 10 km then simulations with $m/k = -3.0$ correspond to a wave packet having horizontal and vertical wavelength of approximately 6 and 2 km, respectively. The nondimensional wave amplitude of $A_{\xi 0}k = 0.05$ corresponds to an initial maximum vertical displacement of 50 m. Weakly nonlinear effects become important after propagating upward 10 km. Although linear theory predicts they become unstable after another propagating upward another 30 km, the simulations (see Fig. 6d) show that they do not first become overturning until propagating upward another 100 km. Of course, these simulations are idealized in that the background is uniformly stratified, unsheared, and steady. But these results serve as a reminder that predictions for wave breaking based on linear theory can be qualitatively unreliable.

Although weakly nonlinear theory well captures the early-time behavior or moderately large-amplitude internal wave packets, fully nonlinear simulations show that overturning occurs as a result of processes not captured by the nonlinear Schrödinger equation. Ultimately, wave overturning predictions should be determined by empirical estimates based on a comprehensive range of fully nonlinear simulations.

We restricted the fully nonlinear model to examine two-dimensional internal waves, and so we did not analyze the process of breaking and momentum deposition in detail because this involves fully three-dimensional turbulence and mixing. However, consistent with our two-dimensional simulations, preliminary simulations using a fully three-dimensional anelastic equation solver indicate that a spanwise-uniform quasi-monochromatic wave packet maintains its two-dimensional structure until breaking (T. Lund, Colorado Research Associates, 2011, personal communication). In future work this code will be used to characterize momentum deposition due to wave saturation. It is hoped that these results will eventually provide a more objective and physically sound justification for gravity wave drag parameterization schemes used presently.

Acknowledgments. This research was supported by the Natural Sciences and Engineering Research Council of Canada (NSERC) and the Canadian Foundation for Climate and Atmospheric Sciences (CFCAS).

APPENDIX

Overturning Conditions

An anelastic gas is negatively buoyant where the potential temperature decreases with height. Where this occurs for anelastic internal waves, we say they are overturning. In terms of the background and fluctuation potential temperature, $\overline{\theta}$ and θ, respectively, the overturning condition is

$$\frac{d\overline{\theta}}{dz} + \frac{\partial \theta}{\partial z} < 0. \tag{A1}$$

Multiplying through by $g/\overline{\theta}$ this condition can be rewritten in terms of the background squared buoyancy frequency (13) and the change ΔN^2 that results from the stretching and compression of isentropes by internal waves.

From the polarization relations (see Table 1), we can recast the overturning condition in terms of the vertical displacement of the waves. In an isothermal atmosphere with density scale height H, the overturning level occurs where

$$z_b = 2H \ln(1/|mA_{\xi 0}|), \tag{A2}$$

in which $A_{\xi 0}$ is the maximum initial vertical displacement arbitrarily set to occur at $z = 0$. It is acceptable to

assess the breaking height of wave packets using the overturning condition for plane waves if the width, σ, of the wave packets is large enough ($|m\sigma| \gg 1$) that any correction to the plane formula is negligible.

To determine where overturning first occurs in numerical simulations, we explicitly compute the minimum value of ΔN^2 at each time step. From the Fourier coefficient of the vorticity field, the polarization relations are used at each time to find the complex-valued amplitude of the potential temperature field $\vartheta(z, t) = \vartheta_r + i\vartheta_i$. The actual fluctuation potential temperature is

$$\theta = \frac{1}{2}\vartheta e^{ikx} + \text{cc}.$$

Extrema to $\partial_z\theta$ occur where $\partial_{zz}\theta = 0$. This occurs where $kx = \tan^{-1}(\vartheta_r''/\vartheta_i'')$, in which primes denote z derivatives. Putting this in the expression for $\partial_x\theta$ gives the minimum value of ΔN^2:

$$\min\Delta N^2 = -\frac{g}{\bar{\theta}}\left[\frac{|\vartheta_r'\vartheta_i'' - \vartheta_i'\vartheta_r''|}{\sqrt{(\vartheta_r'')^2 + (\vartheta_i'')^2}}\right]. \qquad \text{(A3)}$$

REFERENCES

Akylas, T. R., and A. Tabaei, 2005: Resonant self-acceleration and instability of nonlinear internal gravity wavetrains. *Frontiers of Nonlinear Physics,* A. Litvak, Ed., Institute of Applied Physics, 129–135.

Benjamin, T. B., and J. E. Feir, 1967: The disintegration of wavetrains on deep water. Part 1: Theory. *J. Fluid Mech.,* **27,** 417–430.

Bretherton, F. P., 1966: The propagation of groups of internal gravity waves in a shear flow. *Quart. J. Roy. Meteor. Soc.,* **92,** 466–480.

Dosser, H. V., and B. R. Sutherland, 2011: Weakly nonlinear non-Boussinesq internal gravity wavepackets. *Physica D,* **240,** 346–356.

Dunkerton, T. J., 1981: Wave transience in a compressible atmosphere. Part I: Transient internal wave, mean-flow interaction. *J. Atmos. Sci.,* **38,** 281–297.

Eliassen, A., and E. Palm, 1961: On the transfer of energy in stationary mountain waves. *Geofys. Publ.,* **22,** 1–23.

Fermi, E., J. Pasta, and S. Ulam, 1974: Studies of nonlinear problems I. *Nonlinear Wave Motion,* A. C. Newell, Ed., American Mathematical Society, 143–156.

Fritts, D. C., and T. J. Dunkerton, 1984: A quasi-linear study of gravity-wave saturation and self-acceleration. *J. Atmos. Sci.,* **41,** 3272–3289.

——, J. R. Isler, and O. Andreassen, 1994: Gravity wave breaking in two and three dimensions. Part 2: Three-dimensional evolution and instability structure. *J. Geophys. Res.,* **99,** 8109–8123.

Grimshaw, R. H. J., 1975: Nonlinear internal gravity waves and their interaction with the mean wind. *J. Atmos. Sci.,* **32,** 1779–1793.

Klein, R., 2009: Asymptotics, structure, and integration of soundproof atmospheric flow equations. *Theor. Comp. Fluid Dyn.,* **23,** 161–195.

Klostermeyer, J., 1982: On parametric instabilities of finite-amplitude internal gravity waves. *J. Fluid Mech.,* **119,** 367–377.

Lindzen, R. S., 1981: Turbulence and stress owing to gravity wave and tidal breakdown. *J. Geophys. Res.,* **86,** 9707–9714.

Lipps, F. B., and R. S. Hemler, 1982: A scale analysis of deep moist convection and some related numerical calculations. *J. Atmos. Sci.,* **39,** 2192–2210.

Lombard, P. N., and J. J. Riley, 1996: On the breakdown into turbulence of propagating internal waves. *Dyn. Atmos. Oceans,* **23,** 345–355.

McFarlane, N. A., 1987: The effect of orographically excited gravity wave drag on the general circulation of the lower stratosphere and troposphere. *J. Atmos. Sci.,* **44,** 1775–1800.

McLandress, C., 1998: On the importance of gravity waves in the middle atmosphere and their parameterization in general circulation models. *J. Atmos. Solar Terr. Phys.,* **60,** 1357–1383.

Ogura, Y., and N. A. Phillips, 1962: Scale analysis of deep and shallow convection in the atmosphere. *J. Atmos. Sci.,* **19,** 173–179.

Palmer, T. N., G. J. Shutts, and R. Swinbank, 1986: Alleviation of a systematic westerly bias in general circulation and numerical weather prediction models through an orographic gravity drag parametrization. *Quart. J. Roy. Meteor. Soc.,* **112,** 1001–1039.

Phillips, O. M., 1981: Wave interactions—The evolution of an idea. *J. Fluid Mech.,* **106,** 215–227.

Scinocca, J. F., and T. G. Shepherd, 1992: Nonlinear wave-activity conservation laws and Hamiltonian structure for the two-dimensional anelastic equations. *J. Atmos. Sci.,* **49,** 5–27.

——, and N. A. McFarlane, 2000: The parameterization of drag induced by stratified flow of anisotropic orography. *Quart. J. Roy. Meteor. Soc.,* **126,** 2353–2393.

Sutherland, B. R., 2001: Finite-amplitude internal wavepacket dispersion and breaking. *J. Fluid Mech.,* **429,** 343–380.

——, 2006a: Internal wave instability: Wave-wave vs wave-induced mean flow interactions. *Phys. Fluids.,* **18,** 074107, doi:10.1063/1.2219102.

——, 2006b: Weakly nonlinear internal gravity wavepackets. *J. Fluid Mech.,* **569,** 249–258.

——, 2010: *Internal Gravity Waves*. Cambridge University Press, 378 pp.

——, and W. R. Peltier, 1994: Turbulence transition and internal wave generation in density stratified jets. *Phys. Fluids,* **6A,** 1267–1284.

Whitham, G. B., 1974: *Linear and Nonlinear Waves*. John Wiley and Sons, 636 pp.